CIHR Author Manuscript

CIHR Author Manuscript

CIHR Author Manuscript

CIHR IRSC Canadian Institutes of Health Research Instituts de recherche en santé du Canada

Submitted by CIHR
Déposé par les IRSC

Bull Math Biol. Author manuscript; available in PMC 2017 March 20.

Published in final edited form as:
Bull Math Biol. 2015 December ; 77(12): 2264–2293. doi:10.1007/s11538-015-0122-4.

Mathematical Model of Cardiovascular and Metabolic Responses to Umbilical Cord Occlusions in Fetal Sheep

Qiming Wang[1], **Nathan Gold**[1], **Martin G. Frasch**[2,3,4], **Huaxiong Huang**[1], **Marc Thiriet**[5], and **Xiaogang Wang**[1]

[1]Department of Mathematics and Statistics, York University, Toronto, ON M3J 1P3, Canada

[2]Department of Obstetrics and Gynecology, Faculty of Medicine, CHU Sainte-Justine Research Center, Montréal, QC H3T 1C5, Canada

[3]Department of Neurosciences, Faculty of Medicine, CHU Sainte-Justine Research Center, Montréal, QC H3T 1C5, Canada

[4]Centre de Recherche en Reproduction Animale (CRRA), Université de Montréal, 3200 rue Sicotte, Saint-Hyacinthe, QC J2S 7C6, Canada

[5]UPMC, Laboratoire Jacques-Louis Lions, CNRS, UMR 7598, INRIA, EPI REO, Sorbonne University, 75252 Paris, France

Abstract

Fetal acidemia during labor is associated with an increased risk of brain injury and lasting neurological deficits. This is in part due to the repetitive occlusions of the umbilical cord (UCO) induced by uterine contractions. Whereas fetal heart rate (FHR) monitoring is widely used clinically, it fails to detect fetal acidemia. Hence, new approaches are needed for early detection of fetal acidemia during labor. We built a mathematical model of the UCO effects on FHR, mean arterial blood pressure (MABP), oxygenation and metabolism. Mimicking fetal experiments, our *in silico* model reproduces salient features of experimentally observed fetal cardiovascular and metabolic behavior including FHR overshoot, gradual MABP decrease and mixed metabolic and respiratory acidemia during UCO. Combined with statistical analysis, our model provides valuable insight into the labor-like fetal distress and guidance for refining FHR monitoring algorithms to improve detection of fetal acidemia and cardiovascular decompensation.

Keywords

Mathematical modeling; Fetal blood circulation; Fetal acidemia; Hemodynamics; Labor; Neural control; Sensitivity analysis

1 Introduction

One of the main issues during childbirth is the possibility of developing severe fetal acidemia (pH < 7.0) caused by umbilical cord occlusions (UCO) due to repetitive uterine

Correspondence to: Huaxiong Huang.

CIHR Author Manuscript CIHR Author Manuscript CIHR Author Manuscript

contractions. The resulting increased risk of ischemic brain injury can be associated with acidemia (Liston et al. 2007). The sudden compression of the umbilical cord leads to fetal hypertension and fetal heart rate (FHR) decelerations, which are mediated through chemoreflex and sympathetic stimulation (Low et al. 1995; Westgate et al. 1999; Bennet et al. 2005). Fetal oxygen delivery via the umbilical cord is interrupted and leads to hypoxemia and acute cerebral hypoxia (Mallard et al. 1995; Koos et al. 1995; Bishai et al. 2003; Hunter et al. 2003; Westgate et al. 2007; Thakor and Giussani 2008). In addition, FHR reduction and oxygen deficiency also activate sympathetic and parasympathetic brainstem centers resulting in changes of afferent and threshold efferent firing rates (Frasch et al. 2009a, 2012). These activities, in turn, via efferent signaling, regulate FHR and systemic arterial blood pressure. Furthermore, prolonged cord compression and/or repeated cord compressions may cause accumulation of metabolites, such as CO_2 and lactate, in the fetus, which contributes to acidemia (Bennet et al. 2005; Frasch et al. 2009b), as well as prolonged cerebral hypoperfusion (Yan et al. 2009). A comprehensive discussion on the dynamic changes of the fetal circulation and blood flow distribution during hypoxia and asphyxia due to different experimental disturbances can be found in the review paper (Jensen et al. 1999).

Beyond the physiological understanding of the general process, a clinically relevant question is how to monitor and predict the levels of fetal acidemia based on the available clinical data so that the fetal brain can be protected by medical intervention. Since direct continuous measurements of acidemia from fetal blood are not possible clinically and measurements can only be done intermittently in an animal model, an attempt has been made to use statistical approaches to make prediction of acidemia based on FHR (Agrawal et al. 2003). However, current FHR-based clinical algorithms do not provide an accurate prediction of acidemia (de Haan et al. 1997). This is because there is no a priori knowledge of which FHR properties best reflect acidemia. Therefore, a mechanistic modeling approach that can identify FHR properties related to acidemia will provide valuable insights that are useful for developing more effective diagnostic tools.

Mathematical modeling and simulation are useful alternatives to experiments, especially when they are too difficult or too expensive. One of the advantages of mathematical models is that they allow us to conduct parametric studies easily—the physical quantities can be easily tracked. A popular mathematical model in describing the cardiovascular system coupled with the central nervous system has been proposed by Ursino (1998), followed by many related studies that can reproduce and predict the cardiovascular responses in various systems successfully (Ursino and Magosso 2000, 2003; Liang and Liu 2006; Liang et al. 2009; van der Hout-van der Jagt et al. 2013). The drawback is that usually the biological system has a large number of parameters, some of which are difficult or impossible to measure. This makes analysis difficult and can easily introduce uncertainties and errors in the model. A similar cardiovascular mathematical model was used to explore physiological mechanisms in postural change and related physiology problems (Olufsen et al. 2004, 2005; Ellwein et al. 2008). These models are based on electric circuit analogs. In addition, Olufsen’s group (Ellwein et al. 2008) also performed a sensitivity analysis to better understand the model’s dynamics and the impact of the parameters on outputs. A recent review of various models can be found in Shi et al. (2011).

CIHR Author Manuscript CIHR Author Manuscript CIHR Author Manuscript

The metabolic dynamics formulated using a deterministic approach are based on the cardiovascular model by Olufsen's group and a similar (local) sensitivity analysis. A regulation model is incorporated to provide cardiovascular feedback with respect to the arterial pressure and substrate (oxygen, lactate, glucose) concentrations via central neural system, following the works in Ursino (1998), Liang and Liu (2006), van der Hout-van der Jagt et al. (2012, 2013). Details are revealed in Sect. 2. Furthermore, the current model incorporates biochemical processes with proper substrate transfer between blood and organs. As indicated by experiments (Westgate et al. 2001; Frasch et al. 2009b), metabolic dynamics are closely related to the development of acidemia in fetal sheep and accumulation of waste, such as CO_2 and lactate, contribute to the decline in pH. A mathematical model can continuously display in both time and space, the evolution of implicated molecular concentrations, unlike experimental measurements.

The present mathematical model consists of three elements: a lumped parameter model for the cardiovascular circuit coupled with nervous regulation and reciprocal perfusion–metabolism influences. This model is used to investigate the effect of UCOs on FHR, MABP pattern and acidemia development. Our model reproduces some of the patterns observed in animal experiments such as FHR overshoot, deceleration, MABP and pH decline, lactate and CO_2 increase. More importantly, we have confirmed correlation between root-mean-square of the successive differences (RMSSD), a statistical measure of FHR variability and critical levels of lactate and pH (Frasch et al. 2009c). On the other hand, we have also shown that one has to be careful when applying RMSSD as a predictive index. In particular, a variable window size should be used to compute RMSSD when the occlusion duration varies instead of blindly applying standard signal processing techniques.

The rest of the paper is organized as follows. The model equations are given in Sect. 2 for different components. In Sect. 3, model calibration is discussed and a sensitivity analysis is carried out to identify the most sensitive parameters in the mathematical model. Numerical results motivated by different fetal experiments are presented in cardiovascular responses in Sect. 3.2 and metabolic dynamics in Sect. 3.3. Statistical analysis based on contingency tables and RMSSD are discussed in Sect. 3.4. Finally, a summary and conclusions are given in Sect. 4.

2 Mathematical Formulation

2.1 Cardiovascular System

Our model includes both maternal and fetal circulations. Similar to previous studies (Olufsen et al. 2004; van der Hout-van der Jagt et al. 2012), we use an electrical circuit analog, where pressure $p(t)$ is analogous to voltage, volumetric flow rate $q(t)$ to the current and compliance C to capacitance. In addition, the resistance R accounts for the pressure drop due to blood viscosity in each element of the circuit. A schematics of the model with individual components is given in Fig. 1. We model the heart (in both maternal and fetal circulation) as an effective left ventricle (Olufsen et al. 2004), which has two ideal valves on two sides. Two compartments are used to model the branching flow before and after the ventricle, where p_a and p_v are computed (Olufsen et al. 2004). Our model hearts are effective pumps that produce the desirable cardiovascular outputs to maintain both maternal and fetal

CIHR Author Manuscript CIHR Author Manuscript CIHR Author Manuscript

blood circulations. The fetal systemic circulation is modeled as one compartment with subscript ‘nc’ (Fig. 1). Whereas the remaining fetal circulation is considered as one compartment, the umbilical cord and cerebral circulation are modeled separately with arteries and veins (van der Hout-van der Jagt et al. 2012). The maternal circulation system is coupled with the fetal circulation system through partial oxygen pressure in intervillous space of the placenta connected to the umbilical cord. We adopt an oxygen transport model (Couto et al. 2002) where the oxygen distribution in the circulatory systems is given by conservation of mass (van der Hout-van der Jagt et al. 2012) including convection, diffusion and reaction (metabolic uptake and consumption) in the circuit. The blood pressure and oxygen content are coupled through a regulatory model on heart rate by the vagal-sympathetic control (Ursino 1998; van der Hout-van der Jagt et al. 2012).

The basic equations predicting blood pressure and flow can be obtained by computing the volume of each compartment $V_i = C_i p_i$, where C_i and p_i are the corresponding compliance and pressure, respectively, and the change of volume in each compartment is then given by

$$\frac{\mathrm{d}V_i}{\mathrm{d}t} = q_{\mathrm{in}} - q_{\mathrm{out}}. \quad (1)$$

where the subscript i stands for a (artery), v (vein), um (umbilical) and c (cerebral; Fig. 1). An analogy to Ohm’s law provides a linear relation between pressure p and flow rates q

$$q_i = \frac{p_{\mathrm{in}} - p_{\mathrm{out}}}{R_i}. \quad (2)$$

In this study, only the resistance in the system is modeled, whereas inertia is neglected (Olufsen et al. 2004). With compliances kept as constants, the equations for pressure change are given by

$$C_i \frac{\mathrm{d}p_i}{\mathrm{d}t} = q_{\mathrm{in}} - q_{\mathrm{out}}. \quad (3)$$

The fetal heart is modeled similarly as the left ventricle used in the study (Olufsen et al. 2004) (a combined ventricle) where the details in pulmonary circulation and the ductus arteriosus are ignored. The rate of volume change and pressure–volume relationship (Olufsen et al. 2004) are given by

$$\frac{\mathrm{d}V_h}{\mathrm{d}t} = {}_{(p_h < p_v)} q_v - {}_{(p_h > p_a)} q_a, \quad (4)$$

CIHR Author Manuscript CIHR Author Manuscript CIHR Author Manuscript

$$p_h = a_h(V_h - b_h)^2 + (c_h(t)V_h - d_h)g_h(t). \quad (5)$$

In Eq. 4, $\mathbb{1}_{(p_h < p_v)}$ and $\mathbb{1}_{(p_h > p_a)}$ are the indicator functions for valves with zero and one for a closed and open valve, respectively. Conservation of the total volume of the system requires that $\frac{\mathrm{d}}{\mathrm{d}t}\sum_{i\in[\mathrm{a,v,um,c,h}]} V_i = 0$ in fetus and $\frac{\mathrm{d}}{\mathrm{d}t}\sum_{i\in[\mathrm{a,v,ut,h}]} V_i = 0$ in mother (Olufsen et al. 2004), where $V_i = C_i\, p_i$. To model the branching before and after the ventricle, the flow rate satisfies the law of mass conservation (Olufsen et al. 2004, 2005; van der Hout-van der Jagt et al. 2012), given by

$$q_a = q_{c,a} + q_{\mathrm{nc}} + q_{\mathrm{um},a}, \quad (6)$$

$$q_v = q_{c,v} + q_{\mathrm{nc}} + q_{\mathrm{um},v}. \quad (7)$$

In Eq. 5, V_h, p_h and $c_h(t)$ are the heart volume, pressure and contractility, respectively. The parameters a_h and b_h are related to the ventricular elastance during relaxation and the ventricular volume for zero diastolic pressure, respectively, whereas c_h and d_h are related to the volume-dependent and volume-independent components of the developed pressure, respectively (Olufsen et al. 2004). Here $g_h(t) = f_h(t)/f_h(t_p)$ is an activation function that controls periodic oscillation. In maternal circulation, $c_{h,m}(t) = c_m$ is assumed to be a constant, whereas in fetal circulation $c_h(t)$ is regulated by β sympathetic activity (see Eq. 34 below) and $f_h(t)$ is given by Olufsen et al. (2004),

$$f_h(t) = \begin{cases} p_p(G)\frac{t^n(\beta(H)-t)^m}{n^n m^m(\beta_h(H)/(m+n))^{m+n}}, & 0 \le t \le \beta_h(H), \\ 0, & \beta_h(H) < t \le T \end{cases}$$

where H is the heart rate controlled by the nervous system (Sect. 2.4), n and m characterize the contraction and relaxation phases, t_p and p_p are the peak time and peak value of the activation and $\beta_h(H)$ is the valve closure time. According to Olufsen et al. (2004), the expressions for t_p, p_p and $\beta_h(H)$ are given by

$$t_p = t_{\min} + \frac{\theta^\nu}{H^\nu + \theta^\nu}(t_{\max} - t_{\min}), \quad (8)$$

$$p_p = p_{\min} + \frac{H^\eta}{H^\eta + \phi^\eta}(p_{\max} - p_{\min}), \quad (9)$$

CIHR Author Manuscript

CIHR Author Manuscript

CIHR Author Manuscript

$$\beta_h(H)=\frac{n+m}{n}t_p(H) \quad (10)$$

where ν and η are parameters that control the steepness of the sigmoidal change. Blood is pumped out from heart into arterial system and flows through each individual compartment such as the umbilical cord, cerebral and systemic compartments in the fetal circulation system, and returns to the heart via the vein (Fig. 1).

2.2 Metabolic Model

The model for oxygen distribution is based on mass conservation (Couto et al. 2002; van der Hout-van der Jagt et al. 2012). Oxygen concentration $[O_2]$ in each compartment is given by the following equations

$$\frac{\mathrm{d}\left([\mathrm{O}_2]_{\mathrm{ivs}}V_{\mathrm{ivs}}\right)}{\mathrm{d}t}=q_{\mathrm{ivs}}([\mathrm{O}_2]_{m,a}-[\mathrm{O}_2]_{\mathrm{ivs}})-S_{\mathrm{O}_2,d}, \quad (11)$$

$$\frac{\mathrm{d}\left([\mathrm{O}_2]_{\mathrm{um}}V_{\mathrm{um}}\right)}{\mathrm{d}t}=q_{\mathrm{um},a}([\mathrm{O}_2]_a-[\mathrm{O}_2]_{\mathrm{um}})+S_{\mathrm{O}_2,d}, \quad (12)$$

$$\frac{\mathrm{d}\left([\mathrm{O}_2]_cV_c\right)}{\mathrm{d}t}=q_{c,a}([\mathrm{O}_2]_a-[\mathrm{O}_2]_c)-\mathrm{O}_{\mathrm{met},c}, \quad (13)$$

$$\frac{\mathrm{d}\left([\mathrm{O}_2]_{\mathrm{nc}}V_{\mathrm{nc}}\right)}{\mathrm{d}t}=q_{\mathrm{nc}}([\mathrm{O}_2]_a-[\mathrm{O}_2]_{\mathrm{nc}})-\mathrm{O}_{\mathrm{met,nc}}, \quad (14)$$

where the subscript ivs stands for the intervillious space. The feeding oxygen concentration in fetus is given by

$$[\mathrm{O}_2]_a=\frac{[\mathrm{O}_2]_{\mathrm{um}}q_{\mathrm{um},a}+[\mathrm{O}_2]_{\mathrm{nc}}q_{\mathrm{nc}}+[\mathrm{O}_2]_cq_{c,a}}{q_a}, \quad (15)$$

whereas $[O_2]_{m,a} = 0.2$ is fixed in the maternal part (Couto et al. 2002). $S_{O_2,d}$ and $O_{met,i}$ account for diffusion and metabolic uptake, respectively (Couto et al. 2002; van der Hout-van der Jagt et al. 2012). The oxygen diffusion in the placenta is determined by the oxygen partial pressure difference between the intervillous space and the umbilical cord (or umbilical microcirculation),

CIHR Author Manuscript CIHR Author Manuscript CIHR Author Manuscript

$$S_{O_2,d}=D(P_{O_2,ivs}-P_{O_2,um}) \quad (16)$$

where P_{O_2} is the partial oxygen pressure and D is the mass transfer coefficient. Oxygen concentration is related to oxygen partial pressure by the following relation (subscripts um, c, nc, ivs are omitted)

$$[O_2]=\frac{\alpha_b Hb_i}{1+c_{1,i}(P_{O_2}^3+c_{2,i}P_{O_2})^{-1}}+\beta_d P_{O_2}, \quad (17)$$

where constant α_b represents the maximum binding capacity of hemoglobin, Hb_i (i = f, m) is the hemoglobin concentration for fetus and mother, and constant β_d is the content of dissolved oxygen, and $c_{1,i}$ and $c_{2,i}$ (i = f,m) are scaling constants. The metabolic uptake in Eqs. 13 and 14 is constant when the oxygen supply is sufficient. When oxygen concentration drops below a threshold concentration, $[O_2]_{th}$, it is assumed to be a linear function of the oxygen concentration. Combining the two, we have

$$O_{met}=\begin{cases} O_{met,0}, & [O_2]\geq[O_2]_{th}, \\ O_{met,0}+K_{th}([O_2]-[O_2]_{th}), & [O_2]<[O_2]_{th} \end{cases}$$

for all fetal compartments (van der Hout-van der Jagt et al. 2012). In maternal circulation, we assume that oxygen supply is sufficient (Couto et al. 2002; van der Hout-van der Jagt et al. 2012).

As an indicator for asphyxia (due to prolonged UCO typically), we model the CO_2 distribution, using the equation for the law of mass conservation for CO_2, in each fetal compartment as follows

$$\frac{d([CO_2]_{um}V_{um})}{dt}=q_{um,a}([CO_2]_a-[CO_2]_{um})+D_{CO_2}(P_{CO_2,ivs}-P_{CO_2,um}), \quad (18)$$

$$\frac{d([CO_2]_c V_c)}{dt}=q_{c,a}([CO_2]_a-[CO_2]_c)+M_c, \quad (19)$$

$$\frac{d([CO_2]_{nc}V_{nc})}{dt}=q_{nc}([CO_2]_a-[CO_2]_{nc})+M_{nc}+M_{pH}, \quad (20)$$

where $[CO_2]_a$ is given by

CIHR Author Manuscript CIHR Author Manuscript CIHR Author Manuscript

$$[\mathrm{CO_2}]_a = \frac{[\mathrm{CO_2}]_{\mathrm{um}} q_{\mathrm{um},a} + [\mathrm{CO_2}]_{\mathrm{nc}} q_{\mathrm{nc}} + [\mathrm{CO_2}]_c q_{c,a}}{q_a}. \quad (21)$$

$D_{\mathrm{CO_2}}$ is the diffusion coefficient, $\mathrm{P_{CO_2}}$ is the partial pressure of carbon dioxide, M_i is the production rate of $[\mathrm{CO_2}]_i$ and M_{pH} is given by

$$M_{\mathrm{pH}} = 0.1 \frac{([\mathrm{H^+}] - 40)^2}{1 + ([\mathrm{H^+}] - 40)^2}. \quad (22)$$

We assume that CO_2 is cleared in the placenta by fixing $\mathrm{P_{CO_2,ivs}}$ = 40 mmHg. In addition, we assume that the production of carbon dioxide is related to the metabolic rate of oxygen and $M_{c(nc)} = K_M \mathrm{O_{met,}}_{c(\mathrm{nc})}$ (Khoo et al. 1991) with a constant K_M (taken to be 0.2 in this study). The partial pressure of carbon dioxide relates to the concentration linearly as Khoo et al. (1982)

$$[\mathrm{CO_2}] = K_{\mathrm{CO_2}} \mathrm{P}_{\mathrm{CO_2}} + k_{\mathrm{CO_2}}, \quad (23)$$

where $K_{\mathrm{CO_2}}$ and $k_{\mathrm{CO_2}}$ are scaling constants.

To assess the acidity level (de Haan et al. 1997; Frasch et al. 2009b; Ross et al. 2013), lactate and pH values usually measured in fetal animal experiments are included in our model (Fig. 2). Following Cabrera et al. (1998) and D'Angelo and Papelier (2005), we consider pyruvate-, glucose- and lactate-related metabolic pathways in the fetal body or systemic compartment, in particular, anaerobic glycolysis, pyruvate reduction, gluconeogenesis, glycogen synthesis and breakdown, lactate oxidation, lactate buffering. The equations for glucose (GL), lactate (LA) and pyruvate (PY), from the literature (D'Angelo and Papelier 2005) which solves a coupling between cardiovascular response and metabolism for excises, are

$$\frac{\mathrm{d}V[\mathrm{GL}]}{\mathrm{d}t} = q([\mathrm{GL}]_a - [\mathrm{GL}]) + m\phi_{\mathrm{GY},b} \frac{\mathrm{PS}}{\mathrm{PS} + k_{\mathrm{GY},b}} [\mathrm{GY}] - \phi_{GL,b} \frac{\mathrm{PS}}{\mathrm{PS} + k^{\mathrm{PS}}_{\mathrm{GL},b}} \frac{[\mathrm{GL}]}{\mathrm{RS}/k^{\mathrm{RS}}_{\mathrm{GL},b} + 1} - \phi_{GY,s} \frac{[\mathrm{GL}]}{\mathrm{PS}/k_{\mathrm{GY},s} + 1}$$

(24)

CIHR Author Manuscript CIHR Author Manuscript CIHR Author Manuscript

$$\frac{\mathrm{d}V[\mathrm{PY}]}{\mathrm{d}t}=q\left([\mathrm{PY}]_a-[\mathrm{PY}]\right)+2\phi_{GL,b}\frac{\mathrm{PS}}{\mathrm{PS}+k^{\mathrm{PS}}_{\mathrm{GL},b}}\frac{[\mathrm{GL}]}{\mathrm{RS}/k^{RS}_{\mathrm{GL},b}+1}$$
$$-\phi_{\mathrm{PY},r}\frac{\mathrm{RS}}{\mathrm{RS}/k_{\mathrm{PY},r}+1}[\mathrm{PY}]-\phi_{\mathrm{PY},o}\frac{\mathrm{RS}}{\mathrm{RS}/k_{\mathrm{PY},o}+1}[\mathrm{PY}]$$
$$+\phi_{LA}\frac{1}{\mathrm{RS}/k_{\mathrm{LA},o}+1}[\mathrm{LA}] \quad (25)$$

$$\frac{\mathrm{d}V[\mathrm{LA}]}{\mathrm{d}t}=q\left([\mathrm{LA}]_a-[\mathrm{LA}]\right)+\phi_{\mathrm{PY},r}\frac{\mathrm{RS}}{\mathrm{RS}/k_{\mathrm{PY},r}+1}[\mathrm{PY}]-\phi_{\mathrm{LA}}\frac{1}{RS/k_{\mathrm{LA},o}+1}[\mathrm{LA}], \quad (26)$$

where V is the compartment volume, whereas q is the corresponding flow rate (subscripts nc, c, um are omitted), the first term on the right-hand side of the equations models convective exchange, $[*]_{\mathrm{in}}$ is the arterial concentration given by Eq. 15, PS = [ADP]/[ATP] and RS = [NADH]/[NAD] are set to 0.13 and 0.11, respectively (Cabrera et al. 1998), [GY] is glycogen concentration, which is much greater than that of the others (Table 2 in Cabrera et al. 1998) and hence is treated as a constant in the current model, ϕ_i are the reaction rates and k_i are constants in compartment denoted by i. The subscripts are short names for different stoichiometry GY, b (GY → mGL), GY, s (mGL → GY), GL, b (GL → 2PY), LA, o (LA → PY) and PY, r (PY → LA).

Close inspection reveals that the kinetic coefficients in front of the substrates are effectively (unknown) constants and we tune them to fit the experimental measurements. Using simplifying notation, we obtain

$$\frac{\mathrm{d}V[\mathrm{GL}]}{\mathrm{d}t}=q\left([\mathrm{GL}]_a-[\mathrm{GL}]\right)+K_1-K_2[\mathrm{GL}], \quad (27)$$

$$\frac{\mathrm{d}V[\mathrm{PY}]}{\mathrm{d}t}=q\left([\mathrm{PY}]_a-[\mathrm{PY}]\right)+K_3[\mathrm{GL}]-K_4[\mathrm{PY}]+K_5[\mathrm{LA}], \quad (28)$$

$$\frac{\mathrm{d}V[\mathrm{LA}]}{\mathrm{d}t}=q\left([\mathrm{LA}]_a-[\mathrm{LA}]\right)+K_6[\mathrm{PY}]-K_5[\mathrm{LA}], \quad (29)$$

where K_i are constants. Constant concentrations for GL, PY, LA are imposed in cerebral and umbilical cord compartments (Table 3). This needs to be modified when asphyxia is fully developed (Yan et al. 2009), which is beyond of the scope of the current paper.

The effect of pH is not included in the lactate Eq. 29, which is modified by adding the production due to deprotonation of lactic acid,

CIHR Author Manuscript CIHR Author Manuscript CIHR Author Manuscript

$$\frac{\mathrm{d}V[\mathrm{LA}]}{\mathrm{d}t}=q\left([\mathrm{LA}]_a-[\mathrm{LA}]\right)+K_6[\mathrm{PY}]-K_5[\mathrm{LA}]+K_{10}[\mathrm{H}^+]. \quad (30)$$

In addition, we add an equation for $[H^+]$ which takes into account two sources of acidity: lactate dehydrogenase and CO_2 accumulation. Under umbilical cord occlusion, experimental evidence shows significant waste accumulation (especially CO_2). We use the following equation in Orlowski et al. (2011)

$$\frac{\mathrm{d}V[\mathrm{H}^+]}{\mathrm{d}t}=q\left([\mathrm{H}^+]_a-[\mathrm{H}^+]\right)+K_7[\mathrm{LA}]+K_8[\mathrm{CO}_2]-K_9, \quad (31)$$

where K_7 and K_8 are coefficients for $[H^+]$ accumulation due to increased level of lactate and CO_2; K_9 accounts for the ATP consumption among other effects, which is assumed to be an effective constant that helps to restore normal $[H^+]$ level.

2.3 Effectors

Following Ursino (1998) and van der Hout-van der Jagt et al. (2013), there are a few effectors in the model. For autoregulation (van der Hout-van der Jagt et al. 2013) in the fetal brain, we use the following equation,

$$\frac{\mathrm{d}R_{c,a}}{\mathrm{d}t}=\frac{R^*_{c,a}-R_{c,a}}{\tau_{\mathrm{Rc}}} \quad (32)$$

where

$$R^*_{c,a}=\frac{R_{c,a,\min}+R_{c,a,\max}\exp\left(\frac{[\mathrm{O}_2]_a-[\mathrm{O}_2]_{a,n}}{k_c}\right)}{1+\exp\left(\frac{[\mathrm{O}_2]_a-[\mathrm{O}_2]_{a,n}}{k_c}\right)} \quad (33)$$

where $R_{c,a,\min} = 0.1R_{c,a,0}$ and $R_{c,a,\max} = R_{c,a,0}$. Once oxygen is low, the reduced resistance will allow more flow to the brain. This acts in the opposite direction as the one in systemic circulation (Eq. 36).

The fetal heart contractility $c_h(t)$ in Eq. 5 is regulated by sympathetic nervous control that targets mainly β-adrenergic receptors with a firing rate $f_{s\beta}$ (Sect. 2.4).

$$\Delta c=G_c\ln\left(\frac{f_{s\beta}-f_{s,\min}+f_{s,1}}{f_{s,1}}\right) \quad (34)$$

CIHR Author Manuscript CIHR Author Manuscript CIHR Author Manuscript

which is set to zero if $f_{s\beta} < f_{s,\min}$.

The venous compliance C_v and resistance R_{nc} (van der Hout-van der Jagt et al. 2013) are regulated by sympathetic nervous system that targets mainly α-adrenergic receptors with a firing rate $f_{s\alpha}$,

$$\Delta C_v = G_v \ln\left(\frac{f_{s\alpha} - f_{s,\min} + f_{s,1}}{f_{s,1}}\right), \quad (35)$$

$$\Delta R_{nc} = \frac{R_{nc,\min} + R_{nc,\max}\exp\left(\frac{f_{s\alpha} - f_{s\alpha,n}}{k_{R_{nc}}}\right)}{1 + \exp\left(\frac{f_{s\alpha} - f_{s\alpha,n}}{k_{R_{nc}}}\right)}. \quad (36)$$

2.4 Afferent/Efferent Pathways

Changes in blood and oxygen partial pressures trigger nervous responses via baro- and chemoreceptors. Their effects on heart rate have been described (Ursino 1998; Liang and Liu 2006; van der Hout-van der Jagt et al. 2013), modified in the present work and incorporated in the model. In particular, the period of heart pumping motion T is given by $T = T_0 + \Delta T_s + \Delta T_{va}$, where $T_0 = \tau_0 + T_{s,0} + T_{va,0}$ with τ_0 an offset term, $T_{s/va,0}$ the baseline values of sympathetic/vagal contribution and ΔT_v, ΔT_s are determined by

$$\frac{d\Delta T_{va}(t)}{dt} = \frac{1}{\tau_{T,va}}\left(-\Delta T_{va}(t) + G_{T,va} f_{va}(t - D_{T,va}) - T_{va,0}\right), \quad (37)$$

$$\frac{d\Delta T_s(t)}{dt} = \frac{1}{\tau_{T,s}}\left(-\Delta T_s(t) + \overline{G}_{T,s} f_s(t - D_{T,s}) + G'_{T,s}\,(f_s - f_{s,0})\right). \quad (38)$$

Here $\tau_{T,va}$ and $\tau_{T,s}$ are the respective time constant, $G_{T,va}$ and $\bar{G}_{T,s}$, $G'_{T,s}$ the gains, $D_{T,va}$ and $D_{T,s}$ the delay of the vagal and sympathetic responses. In the results presented in this paper, they are set to zero. At equilibrium state, the second and third terms in the right-hand side of Eqs. 37 and 38 vanish, which leads to $\Delta T_{va} \to 0$ and $\Delta T_s \to 0$, so that the baseline period is recovered at $T = T_0$. Finally, f_{va} and f_s are given by

$$f_{va} = W_{br,va}\frac{f_{va,\min} + f_{va,\max}\exp\frac{f_{br} - f_{br,n}}{k_v}}{1 + \exp\frac{f_{br} - f_{br,n}}{k_v}} + W_{cr,va} f_{cr} + f_{hy}, \quad (39)$$

CIHR Author Manuscript CIHR Author Manuscript CIHR Author Manuscript

$$f_s = \ln\left(\frac{f_{s\beta} - f_{s,\min} + f_{s,1}}{f_{s,1}}\right), \quad (40)$$

with

$$f_{hy} = \frac{f_{hy,\min} + f_{hy,\max}\exp\frac{P_{O_2,c} - P_{O_2,c,0}}{k_{hy}}}{1+\exp\frac{P_{O_2,c} - P_{O_2,c,0}}{k_{hy}}} - f_{va,o}, \quad (41)$$

$$f_{s\alpha(s\beta)} = f_{s,\infty} + (f_{s,0} - f_{s,\infty})\exp k_s\left(-W_{br,s\alpha(s\beta)}\, f_{br} + W_{cr,s\alpha(s\beta)}\, f_{cr} - f_{s\alpha(s\beta),o}\right), \quad (42)$$

where f_{br} and f_{cr} are the afferent baro- and chemoreceptor firing rates, respectively, and $f_{s\alpha(s\beta),o}$ is the hypoxia offset that creates a threshold for sympathetic response. In addition, $f_s = 0$ when $f_{s\beta/s\alpha} < f_{es,\min}$, and $f_s = f_{s,\max}$ when $f_{s\alpha(s\beta)}$ exceeds a threshold value $f_{s,\max}$. Furthermore, the baro- and chemoreceptors afferent firing rates f_{br} and f_{cr} are governed by the following first-order ODE (van der Hout-van der Jagt et al. 2013)

$$\frac{d f_{br}}{dt} = \frac{f_{br}^* - f_{br}}{\tau_{br}}, \quad \frac{d f_{cr}}{dt} = \frac{f_{cr}^* - f_{cr}}{\tau_{cr}}, \quad \frac{d\bar{p}_a}{dt} = \frac{p_a - \bar{p}_a}{N_p} \quad (43)$$

where according to Magosso and Ursino (2001)

$$f_{br}^* = \frac{f_{br,min} + f_{br,\max}\exp\frac{\bar{p} - p_n}{\tau_{pr,br}}}{1+\exp\frac{\bar{p}_a - p_n}{\tau_{pr,br}}}, \quad (44)$$

$$f_{cr}^* = \frac{f_{cr,\max} + f_{cr,\min}\exp\frac{P_{O_2,a} - P_{O_2,n}}{\tau_{pr,cr}}}{1+\exp\frac{P_{O_2,a} - P_{O_2,n}}{\tau_{pr,cr}}}\left(\bar{K}\ln\left(\frac{P_{CO_2,nc}}{P_{CO_2,nc,n}}\right)+1\right), \quad (45)$$

$$\bar{p}_a = \frac{1}{N_p}\int_0^t p_a(s)\exp\left(-\psi(t-s)\right)ds, \quad (46)$$

where $\bar{p}_a$ is the mean arterial blood pressure (MABP) and $f_{br,\max}$, $f_{br,\min}$, $f_{cr,\max}$, $f_{cr,\min}$, $\bar{K}$, p_n, $P_{CO_2,n,nc}$, $P_{O_2,n}$, $\tau_{pr,br}$, $\tau_{pr,cr}$, ψ are constants. The formula used in van der Hout-van der

CIHR Author Manuscript CIHR Author Manuscript CIHR Author Manuscript

Jagt et al. (2013) is recovered when P_{CO_2},nc is in the normal range and f_{cr} rises when P_{CO_2}, nc increases. Unless otherwise stated, $\bar{K} = 1$.

The normalization factor N_p is introduced to ensure that the correct mean arterial blood pressure is calculated (Olufsen et al. 2004),

$$N_p = \int_0^t \exp\left(-\psi(t-s)\right) \mathrm{d}s = \frac{1-\exp\left(-\psi t\right)}{\psi}. \quad (47)$$

The offset value $f_{s\beta/s\alpha,o}$ in Eq. 42 is determined by

$$\frac{\mathrm{d}\, f_{s\alpha(s\beta),o}}{\mathrm{d}t} = \frac{f^*_{s\alpha(s\beta),o} - f_{s\alpha(s\beta),o}}{\tau_s} \quad (48)$$

where

$$f^*_{s\alpha(s\beta),o} = \frac{f_{s\alpha(s\beta),\min} + f_{s\alpha(s\beta),\max} \exp\left(\frac{P_{O_2,a} - P_{O_2,a,n}}{k_{pr,s}}\right)}{1+\exp\left(\frac{P_{O_2,a} - P_{O_2,a,n}}{k_{pr,s}}\right)}. \quad (49)$$

Due to hypoxemia in fetal circulation, the vagal firing rate increases, hence decreasing FHR. The sympathetic response has the opposite effects (Frasch et al. 2009a, c).

To take into account the apparent mutual inhibition of sympathetic and vagal nerves, we model the sympathetic gain $\bar{G}_{T,s}$ as a sigmoidal function of vagal firing rate f_{va},

$$\bar{G}_{T,s} = \frac{\delta G_T \exp\frac{f_{va} - f_{va,n}}{\tau_{gs}}}{1+\exp\frac{f_{va} - f_{va,n}}{\tau_{gs}}}, \quad (50)$$

which shows the sympathetic gain tends to the minimal value as the vagal firing rate increases due to the inhibition effect as mentioned. Similarly, we introduce the following for the vagal gain $G_{T,va}$

$$G_{T,va} = G_{T,va,0} + \frac{G_{T,va,\min} \exp\frac{f_{s\beta} - f_{s\beta,n}}{\tau_{gv}}}{1+\exp\frac{f_{s\beta} - f_{s\beta,n}}{\tau_{gv}}}, \quad (51)$$

where $G_{T,va,min} = 0.1 G_{T,va,0}$. It was pointed out (Kubota et al. 1992a, b; Levy and Zieske 1969) that the gains may depend on pressure and other dynamic variables. For simplicity, they are chosen as constants in the current model. We assume that the sympathetic and vagal

CIHR Author Manuscript

CIHR Author Manuscript

CIHR Author Manuscript

activities in system are mutually inhibitory and mediated via the chemoreceptors and baroreceptors (see Eqs. 50 and 51), which is consistent with physiological explanations (Westgate et al. 2007).

In summary, the above set of 30 ordinary differential equations form a coupled system. Due to the nonlinear nature of the equations, they are solved numerically using MATLAB solver ode15s and subroutines sens_sys and sens_ind, which are given in Breit (2004), for sensitivity analysis. Because of the stiffness of the system, ode15s is chosen over other solvers.

3 Results and Discussion

Two control parameters are used to measure UCO severity: 1) the ratio between the occlusion and the recovery durations and 2) the occlusion degree (partial or complete). As we show below, the effects of these parameters on FHR are significant.

3.1 Model Calibration: Baseline Values and Sensitivity Analysis

As in many cardiovascular models (Ursino 1998; Olufsen et al. 2004; van der Hout-van der Jagt et al. 2012), the parameter space is large. Most of the parameter values are obtained from the literature and the remaining ones are calibrated by comparing our model outputs with available experiments. For example, $G_{T,\mathrm{va},0} \sim 0.04$ is taken instead of 0.09 used for the adult model (Ursino 1998; van der Hout-van der Jagt et al. 2012) to reflect the fact that the vagal control in fetus is not as mature. $G'_{T,s}$ and δG_T are tuned to achieve a reasonable reduction in FHR for fetus. The values of adjusted parameters are given in Tables 1, 2 and 3.

3.1.1 Baseline Case—Several important and clinically relevant quantities are listed in Table 4, which is the baseline case used for model calibration. The predicted values from our model are consistent with experimental data. At the onset of a complete UCO, the flow rate in umbilical cord $q_{\mathrm{fs},a} = q_{\mathrm{fs,va}} = 0$ and O_2 exchange $S_{\mathrm{O2,d}} = 0$ in the corresponding transport equations (Sect. 2). The flow is stopped in the umbilical cord compartment and O_2 and CO_2 cannot be delivered continuously between placental and fetal circulations. Mild and moderate UCOs represent partial occlusions, where the passed flow is set to be 50 and 25 % of the normal case, respectively (Ross et al. 2013). The severe case is referred to as the complete occlusion regarding the degree of occluder.

From an experimental point of view, FHR and MABP are two important quantities often used in modeling and monitoring fetal acidemia, with FHR being the single quantity available clinically. One important feature of FHR in experiments with repetitive UCOs is its significant drop during occlusions. In our model, it is assumed that the sympathetic and vagal activities are mutually inhibitory and mediated via baro- and chemoreceptors (Eqs. 50, 51) (Westgate et al. 2007). FHR does not change markedly when these mechanisms are blocked (van der Hout-van der Jagt et al. 2013).

FHR overshoot and MABP decline are determined by systemic vascular resistance, myocardial contractility and venous compliance under the central nervous control as proposed in the literature (van der Hout-van der Jagt et al. 2013). We tune the parameters G_c

CIHR Author Manuscript CIHR Author Manuscript CIHR Author Manuscript

and G_{va} in Eqs. 34 and 35 for the myocardial contractility and venous compliance, respectively, to achieve FHR overshoot and MABP decline comparable to experimental data. In most cases, sufficient control is achieved with $G_{va} = 0$; namely, the venous compliance is chosen as a constant (Olufsen et al. 2004). However, for 1:5 UCO, a nonzero G_{va} is used to reproduce experimental data (Westgate et al. 1999, 2001).

3.1.2 Sensitivity Analysis—We carry out a local sensitivity analysis on model parameters according to Ellwein et al. (2008), using MATLAB subroutines, sens_sysand sens_ind (Breit 2004).

Suppose the system of equations can be written as

$$\frac{\mathrm{d}\boldsymbol{X}}{\mathrm{d}t}=F(\boldsymbol{X},t,\boldsymbol{p}), \quad (52)$$

where $\boldsymbol{X}$ denotes the state variables and $\boldsymbol{p} = [p_1, p_2, \ldots p_n]$ stands for the parameters. Then the relative sensitivity matrix is defined as

$$S_{ij}(t,\boldsymbol{p})|_{\boldsymbol{p}=\boldsymbol{p}_0}=\frac{\partial \boldsymbol{X}_i(t,p)}{\partial p_j}\frac{p_j}{X_i(t,p)}|_{p=p_0}, \quad p_j, X_i \neq 0. \quad (53)$$

We compute a maximum relative sensitivity

$$\boldsymbol{S}_j=\max_i\left(\max_t S_{ij}(t,p)\right)|_{\boldsymbol{p}=\boldsymbol{p}_0}. \quad (54)$$

We conduct simulations over a period of 500 s without occlusion during which data were recorded. A representative ranking of parameter sensitivity (Fig. 3) illustrates the distribution of most to least sensitive parameters for a numerical test with 70 selected parameters. Unique identification of a full set of parameters appears to be time-consuming and difficult (Ellwein et al. 2008). Some parameters appearing in the regulation model are most sensitive. Many kinetic coefficients appear to be less sensitive (Gui et al. 2015Table 5 with their effects.

Our simulation approach differs from that of Ellwein et al. (2008), in which high-quality data were available. In that case, an optimization procedure is used to fit model output to experimental data. The sensitivity analysis further helps to reduce the computational cost as optimizing the most sensitive parameters suffices to obtain robust results. Unfortunately, we do not have high-quality experimental data as in Olufsen et al. (2004) at this stage. Our sensitivity analysis can only point out the most important controlling parameters that can guide potential future experiments.

CIHR Author Manuscript CIHR Author Manuscript CIHR Author Manuscript

3.2 Cardiovascular Dynamics: FHR and MABP Behavior

We studied the 1-min occlusion scenario, a clinically relevant case. The recovery time for 1-min complete occlusion, that is, the UCO frequency, influences the system behavior significantly. Based on our *in silico* experiments, for 1:2.5 UCO, FHR overshoot appears after about two and half hours with developing acidosis, as demonstrated in vivo (Westgate et al. 1999, 2001; Bennet et al. 2005). In contrast, 1:5 UCO scenario does not show any significant FHR overshoots and acidosis, as shown in the literature (Westgate et al. 2001). The numerical results displayed in Fig. 4 show the typical time variations of FHR and MABP at the early and late stages of occlusion, respectively. For 1:2.5 UCO, FHR deceleration appears once the occlusion begins. The pronounced FHR overshoot occurs only after a delay of approximately 3 h, in agreement with experiments (Westgate et al. 2001). This is accompanied by an eventual decline in MABP after approximately 2 h. At the early stage of the occlusions, MABP rises as soon as the occlusion starts (de Haan et al. 1997; Bennet et al. 2005). The inset in the bottom panel of Fig. 4 (for 1:5 UCO) shows that MABP rises during each occlusion period, even after numerous repetitive occlusions, as expected, but this initial rise tends to disappear in 1:2.5 UCO (left bottom panel). This is again in agreement with experiments (Frasch et al. 2011), as hypotension is expected when pH drops below 7.2. The difference in 1:5 and 1:2.5 UCOs indicates that with sufficient time for recovery, the regulation of effectors is able to maintain the blood pressure level and avoid instability. The detailed mechanism is still unknown and in the real situation, the regulatory functions represented by Eqs. 34 and 35 may depend on time-dependent or memory-related factors. Overall, the results in Fig. 4 demonstrate a reasonable agreement between experimental and numerical data. We will compute the correlation of FHR, MABP and acidosis in Sect. 3.4, as well as the output of the metabolic model.

In addition, intermediate rise occurs typically in FHR and MABP in each occlusion for 1:2.5 UCO, when the FHR overshoot is pronounced. Similar intermediate rise was reported in Westgate et al. (1999), where in the UCO 1:2.5 group, FHR initially recovers after the occlusion, but rapidly falls again before returning to the baseline value eventually. In our case, the trend is similar, but it appears earlier than experiments, with a relatively larger magnitude. We suspect this is caused by some system delay factor. Eqs. 37 and 38 contain delay variables $D_{T,\mathrm{va}}$ and $D_{T,s}$. These are set to zero here because: 1. the delay model in the literature was developed for adults and the correct parameter values are unknown for fetuses; 2. computational cost is much higher for a delayed differential equation system for 4-h simulations than a few minutes as in Olufsen et al. (2004). In addition, this transient growth due to delay does not seem to affect the general feature of our model outcome including the metabolic dynamics (reported below).

Figure 5 displays the numerical results of FHR and MABP for variable UCOs. Complete UCO with varying frequency was motivated by experiments carried out in Frasch et al. (2009b). The FHR overshoot occurs only after a delay of more than 2 h for the 1:2 UCOs, and MABP declines from the second hour for 1:3 UCOs. This is consistent with Fig. 4, in that relatively small frequency UCOs promote the MABP decline and FHR overshoot. Constant frequency UCOs with varying degrees mimic experiments in Frasch et al. (2009c). Mild occlusion has little effect, but moderate occlusion decreases FHR (~10 mmHg) to a

CIHR Author Manuscript

CIHR Author Manuscript

CIHR Author Manuscript

lesser extent to complete UCOs (~70 mmHg). As in Frasch et al. (2009c), after 2 h of severe UCOs, pH drops below 7.0. Therefore, the FHR overshoot instability may be correlated with the worsening acidemia.

3.3 Metabolic Dynamics

To assess the fetal acidemia, a simplified metabolic model is coupled with the cardiovascular model to evaluate pH as well as BD defined by Eq. 55 (see also Frasch et al. 2009b)

$$\mathrm{BD} = -\left(0.02786 \mathrm{P}_{\mathrm{CO}_2} 10^{\mathrm{pH}-6.1} + 13.77\mathrm{pH} - 124.58\right). \quad (55)$$

In particular, we computed the variations of lactate, $[H^+]$ and P_{CO_2} in the systemic compartment to compare with the experimental data.

Figure 6 shows several experimentally measurable quantities over 4-h occlusions. Agreement is shown when comparing with the data extracted from Bennet et al. (2005). Corresponding to the FHR overshoot instability for 1:2.5 UCO in Fig. 4, we find that pH drops below 7.00 and lactate accumulates beyond 10 mM. On the other hand, pH remains in the normal range for 1:5 UCOs, even after four hours of repeated occlusions (Westgate et al. 2001; Bennet et al. 2005). pH, lactate and P_{CO_2} remain close to baseline values. The results depicted in Fig. 7 for variable UCOs captured the experimental data trend. Relatively low-frequency UCOs and completely occluded UCOs have greater influence than those with higher frequency or partially occluded UCOs. Fetal acidosis occurs for severe UCOs, indicated by the BD values and FHR overshoot instability. In an attempt to quantify the relationship of these variables, we compute the correlations between relevant quantities in Sect. 3.4.

3.4 Statistical Analysis

We begin this section by computing a contingency table for each case discussed earlier. In order to make a direct comparison with experimental data, we also present some analysis on RMSSD, an index of vagal modulation of heart rate variability.

We examined correlations between acidemia quantified by BD and lactate on one hand and FHR and MABP on the other. Due to the cyclical nature and time dependency, classical Pearson correlation is not applicable to the data considered here. Therefore, we discretize the original signal into binary time sequences with 1 indicating the occurrence of an anomaly and 0 otherwise. An anomaly is defined as an event when an observation occurs outside an estimated confidence interval of long-term average. We use the mean $\tilde{\mu}$ and standard deviation $\tilde{\sigma}$ to set a threshold value, $\tilde{\mu} \pm 2\tilde{\sigma}$, in order to sort out the relevant quantities. For example, when the FHR (or BD or lactate) is larger than the upper bound threshold value $\tilde{\mu} + 2\tilde{\sigma}$, these quantities are set to 1, otherwise to zero. Similarly, when MABP is smaller than the lower bound of the threshold value $\tilde{\mu} - 2\tilde{\sigma}$, the MABP is set to 1, otherwise to zero. Contingency tables are then constructed for each pair based on the simultaneous occurrence of 1s and 0s.

CIHR Author Manuscript

CIHR Author Manuscript

CIHR Author Manuscript

For 1:2.5 UCOs, representative tables are constructed by taking the last two hours of simulation data, given in Table 6. The counts in each cell record the total number of occurrence for one combination between two discretized time sequences. For example, the first cell in each table records the total numbers of normal occurrence in both time series.

To search possible correlations among FHR, MABP, lactate and BD, two statistical tests are carried out. The first is the traditional Chi-square test, and the second is on the odds ratio derived from each contingency table. Both tests reject the hypothesis that these variables are independent with very small p values ($p < 0.0001$). Therefore, we conclude that the anomalies in these sequences are indeed correlated with each other. The same conclusion can be drawn for UCOs with varying frequencies (Table 7). These findings are consistent with our results in Sects. 3.2 and 3.3, as FHR overshoot, MABP decline and lactate level increase becomes significant when large BD value appears near the end of the occlusions.

However, our results from Table 8 for UCOs with variable occlusion degrees suggest that contingency tables alone may not be sufficient to reveal the subtle relationship among FHR, MABP and BD. Following Frasch et al. (2009a, c), Durosier et al. (2014) via Eq. 56, we compute RMSSD based on our FHR output

$$\mathrm{RMSSD}=\sqrt{\frac{1}{N-1}\left(\sum_i D_i\right)}, \quad (56)$$

where $D_i = |P_{i+1} - P_i|^2$ with P_i the period between two maximum peaks and N is the number of intervals within a certain window. For the case in the left column of Fig. 8, where the frequency is varying, the computed RMSSD qualitatively captures the trend of experimental data, which is displayed in the bottom panel (the discrepancy in magnitude is due to sampling frequency). As the occlusion proceed, RMSSD increases monotonically. The contingency tables do not exhibit significant correlation for this case. However, based on our pH and BD results, we obtain significant increase in RMSSD when acidosis occurs, compared to the baseline values.

In contrast, RMSSD is overestimated for moderate occluded UCOs as soon as occlusion occurs (middle right panel using 5-min window as indicated by the dashed line), whereas no obvious increase is observed afterward. This is similar to a representative set of experimental data (Wang et al. 2014) (bottom right panel).

Interestingly, if we reduce the window size, the computed RMSSD evolves very differently. For example, RMSSD using a 3-min window (cross-symbols, middle right panel of Fig. 8) gradually increases as UCOs proceed and acidosis develops. This suggests that, in addition to the importance of sampling frequency (Durosier et al. 2014), a proper window size is also important.

4 Concluding Remarks

We have investigated the cardiovascular and metabolic responses to UCOs in a fetal sheep circulation system using a mathematical model. Our model comprises a cardiovascular

CIHR Author Manuscript CIHR Author Manuscript CIHR Author Manuscript

circuit, a simplified metabolic model, and neural control of blood pressure and oxygen content by baro- and chemoreceptors (Ursino 1998; van der Hout-van der Jagt et al. 2012, 2013). Waste accumulation in the systemic compartment, such as CO_2 and lactate, is solved simultaneously with the cardiovascular response.

Our mathematical model produces the pattern observed in animal experiments, including FHR decrease and overshoot, MABP and pH decline, and increased levels of lactate and CO_2. In particular, the development of the cardiovascular and metabolic responses in our model are the result of sufficiently long-lasting repetitive occlusions. In other words, acidosis depends on the total duration of occlusion rather than on an individual event, as in de Haan et al. (1997). In addition, the FHR decrease, FHR overshoot and MABP response evolve accordingly to observations obtained using various experimental scenarios. In particular, our results from 1:5 and 1:2.5 UCO demonstrate the possibility that properly functioning effectors (cardiac contractility, systemic resistance and venous compliance) are able to main the blood pressure level and avoid instabilities in FHR. Our simplified metabolic model reproduces measured changes in pH, lactate and glucose. Although expected correlation between FHR overshoot, MABP decline and acidosis (quantified by BD) can be obtained when the occlusion is complete, our results suggest that the correlation analysis may fail when the UCO degree varies significantly. In that case, we show RMSSD is able to qualitatively predict acidemia.

The choice of window size is important in computing RMSSD when UCO frequency varies. Uterine contractions during labor vary in frequency and degree. Therefore, the usual choice of fixed window size may affect the results obtained in Durosier et al. (2014), in addition to the sampling frequency. A proper combination of FHR monitoring and RMSSD computation may then be used to detect acidemia.

One limitation of our model is that, as other mathematical biology models in the literature, the parameter space is large, despite our effort to keep the model simple. Although sensitivity analysis has been carried out, physiological parameters are difficulty to estimate accurately. We plan to use statistical modeling to control the uncertainty in parameters in future work (Ramsay et al. 2007). Another limitation pertains to the simplified metabolic process. A more detailed model will potentially improve predictions of impaired nutrient supply (Cloutier et al. 2009). The transport equations are used with relatively simple kinetic reaction terms involving only O_2, CO_2, pyruvate, lactate, glucose and $[H^+]$ in the systemic compartment. Nevertheless, more experimental data will be needed to properly model the kinetics and regulation.

Acknowledgments

The authors are grateful to Dr. Josh Chang for some useful discussions. This work is partially supported by MITACS, NeuroDevNet, NSERC, CIHR and the Fields Institute.

Abbreviations

FHR	Fetal heart rate
MABP	Mean arterial blood pressure

CIHR Author Manuscript CIHR Author Manuscript CIHR Author Manuscript

UCO	Umbilical cord occlusions
BD	Base deficit
RMSSD	Root-mean-square of the successive differences

List of Symbols

a_h	Coefficient related to ventricular elastance during relaxation (mmHg/ml^2)
a_b	Maximum binding capacity of hemoglobin (ml O_2/g Hb)
b	Parameter related to ventricular volume for zero diastolic pressure (ml)
β_d	Scaling factor on dissolved oxygen (1/mmHg)
$\beta_h(H)$	Time for the onset of ventricular relaxation (s)
η	Parameter controlling the steepness of the relation for heart pressure
θ	Median value of time for peak pressure in heart model (1/s)
ϕ	Median value of heart pressure in heart model (1/s)
ψ	Scaling factor in mean arterial pressure (1/s)
$[CO_2]_i$	Carbon dioxide concentration in compartment i = nc, c, um (ml CO_2/ml blood)
$[CO_2]_a$	Feeding Carbon dioxide concentration in fetus (ml CO_2/ml blood)
c_f, c_m	Heart contractility for fetus/mother (mmHg/ml)
$c_{1,m}, c_{1,f}$	Scaling constant in the relation between Oxygen content and its partial pressure for mother and fetus (mmHg^3)
$c_{2,m}, c_{2,f}$	Scaling constant in the relation between Oxygen content and its partial pressure for mother and fetus (mmHg^2)
C_i	Compliance in compartment i = nc, c, um, ut (ml/mmHg)
d_f, d_m	Parameter related to the volume-dependent and volume-independent components of the developed pressure (mmHg)
δG_T	Scaling factor for sympathetic gain (s^2)
D	Mass transfer coefficient in Oxygen model (ml O_2/s/mmHg)

CIHR Author Manuscript CIHR Author Manuscript CIHR Author Manuscript

D_{CO_2}	Mass transfer coefficient in Carbon dioxide model (ml CO_2/s/mmHg)
ΔC_v	Effector in venous compliance (ml/mmHg)
Δc	Effector in heart contractility (mmHg/ml)
f_{br}, f_{cr}	Afferent firing rate via stimulation of baro/chemoreceptor (1/s)
$f_{i,o}$	Offset values that create a threshold for vagal or sympathetic response i = va, $s\beta$, $s\alpha$ (1/s)
$f_{i,min}$, $f_{i,max}$	Control constants in sigmoid functions i = s, va, hy, br, cr (1/s)
$f_{i,n}$	A normal value for corresponding afferent or efferent firing rate i = br, cr, va, $s\beta$, $s\alpha$ (1/s)
$f_{s,0}$, $f_{s,\infty}$	Constants in sympathetic firing rate function (1/s)
$f_{s\beta}$, $f_{s\alpha}$	Efferent α- and β- sympathetic firing rate (1/s)
$f_{s,1}$	Control parameter in sympathetic firing rate function (1/s)
f_{va}	Efferent vagal firing rate (1/s)
G_i	Gain constants i = T_{va}, T_s (s^2)
G_c, G_{va}	Constants in effectors (mmHg s/ml)
$[GL]_a$	Arterial glucose concentration (mM)
$[GL]_i$	Glucose concentration in compartment i = nc, c, um (mM)
$g(t)$	Activation function in heart model
H (FHR)	Heart rate (1/s)
$[H^+]_a$	Arterial proton concentration (nM)
$[H^+]_i$	Proton concentration in compartment i = nc, c, um (nM)
Hb_f, Hb_m	Hemoglobin concentration in fetus or mother (g Hb/ml blood)
K_f	Constant in Oxygen metabolic model (ml blood/s)
K_1	Kinetic constant (mmol/s)
K_i	Kinetic constant i = 2, 3, 4, 5, 6 (ml/s)
K_7	Kinetic constant (10^{-6} ml/s)
K_8, K_9	Kinetic constant (nmol/s)

CIHR Author Manuscript CIHR Author Manuscript CIHR Author Manuscript

K_{10}	Kinetic constant (10^6 ml/s)
K_{CO_2}	Scaling constants (ml CO_2/ml blood/mmHg)
k_{CO_2}	Scaling constants ml (CO_2/ml blood)
k_c	Control constant
k_{hy}, $k_{pr,s}$	Control constant (mmHg)
k_i	Constant $i = R_{nc}$, br, cr, s, va (1/s)
$[LA]_a$	Arterial lactate concentration (mM)
$[LA]_i$	Lactate concentration in compartment i = nc, c, um (mM)
M_i	Production rate of $[CO_2]_i$ with i = nc, c, um (ml/s)
M_{pH}	Production rate due to $[H^+]$ accumulation (ml/s)
N_p	Normalization factor (s)
ν	Parameter related to steepness of the time for peak pressure in heart model
m, n	Parameters related to the onset time of ventricular relaxation in heart model
$[O_2]_{th}$	Threshold value to control Oxygen metabolic uptake (ml O_2/ml blood)
$[O_2]_a$, $[O_2]_{m,a}$	Feeding Oxygen concentration in fetus and mother (ml O_2/ml blood)
$[O_2]_{a,n}$	A normal value to control the sigmoid function in systemic resistance (ml O_2/ml blood)
$[O_2]_i$	Oxygen concentration in compartment i = nc, c, um, ivs (ml O_2/ml blood)
$O_{met,i}$	Metabolic Oxygen uptake in compartment i = nc, c (ml O_2/s)
p_{min}, p_{max}	Control constants in heart model (mmHg)
p_i	Blood pressure in compartment i = nc, c, um, h, ut, ivs (mmHg)
$\bar{p}_a$ (MABP)	Mean arterial blood pressure (mmHg)
$P_{O_2,i}$	Oxygen partial pressure in compartment i = nc, c, um, ivs (mmHg)

CIHR Author Manuscript CIHR Author Manuscript CIHR Author Manuscript

$\mathbf{P_{CO_2,i}}$	Carbon dioxide partial pressure in compartment i = nc, c, um (mmHg)
$\mathbf{P_{CO_2}}$**,nc, n**	A normal value for Carbon dioxide partial pressure in systemic compartment (mmHg)
$\mathbf{P_{O_2,\ c,0}}$	Threshold value for cerebral Oxygen partial pressure to control the sigmoid function in firing rate function f_{hy} (mmHg)
$\mathbf{[PY]_a}$	Arterial pyruvate concentration (mM)
$\mathbf{[PY]_i}$	Pyruvate concentration in compartment i = nc, c, um (mM)
$q_{i,a}$	Arterial flow rate into compartment i = nc, c, um (ml/s)
$q_{i,v}$	Venous flow rate out of compartment i = nc, c, um (ml/s)
$q_{\text{in}}, q_{\text{out}}$	Flow rate in/out of corresponding compartment by summing over flow rate from local branches (ml/s)
R_i	Resistance in compartment i = nc, c, um, ut, ivs, m (mmHg s/ml)
$R_{c,a,0}, R_{cn,0}$	Baseline values for cerebral and systemic resistance (mmHg s/ml)
$R_{c,\text{min}}, R_{c,\text{max}}$	Constants in cerebral autoregulation model (mmHg s/ml)
$R_{\text{nc,min}}, R_{\text{nc,max}}$	Constants in systemic resistance model (mmHg s/ml)
ΔR_{nc}	Effector in systemic resistance (mmHg s/ml)
$S_{i\,j}$	Relative sensitivity matrix
$S_{[O_2],d}$	Oxygen diffusion (ml O_2/s)
$S_{P[O_2]}$	Scaling function to relate Oxygen content and its partial pressure
$s_{\text{mv}}, s_{\text{av}}$	Indicator function of mitral/aortic valve
t_{p}	Peak time (s)
$t_{\text{min}}, t_{\text{max}}$	Control constants in heart model (s)
T_0	Base line value for heart period (s)
$T_{v,0}, T_{s,0}$	Contributions from vagal and sympathetic activities on the base heart period (s)
τ_i	Control constant i = gs, gv (1/s)
τ_0	Offset constant in heart period (s)

$\tau_{pr,br}$, $\tau_{pr,cr}$	Control constant (mmHg)
τ_{br}, τ_{cr}, τ_{s}, τ_{Rc}	Time constant (s)
$\tau_{T,s}$, $\tau_{T,v}$	Time constant (s)
ΔT_s, ΔT_{va}	Contribution to heart period from sympathetic/vagal activity (s)
V_i	Volume in compartment i = nc, c, um, h, ut (ml)
V_{total}	Total volume of all compartments in the circulation system (ml)
$W_{br,i}$, $W_{cr,i}$	Weight factor $i = s\alpha, s\beta$

References

Agrawal S, Doucette F, Gratton R, Richardson B, Gagnon R. Intrapartum computerized fetal heart rate parameters and metabolic acidosis at birth. Obstet Gynecol. 2003; 102:731. [PubMed: 14551003]

Bennet L, Westgate J, Liu Y, Wassink G, Gunn A. Fetal acidosis and hypotension during repeated umbilical cord occlusions are associated with enhanced chemoreflex responses in near-term fetal sheep. J Appl Physiol. 2005; 99:1477. [PubMed: 15976361]

Bishai J, Blood A, Hunter C, Longo L, Power G. Fetal lamb cerebral blood flow (CBF) and oxygen tensions during hypoxia: a comparison of laser Doppler and microsphere measurements of CBF. J Physiol. 2003; 456:869.

Breit, M. Master's thesis. University for Health Sciences, Medical Informatics and Technology; Germany: 2004. Sensitivity analysis of biological pathways.

Cabrera M, Saidel G, Kalhan S. Role of O_2 in regulation of lactate dynamics during hypoxia: mathematical model and analysis. Ann Biomed Eng. 1998; 26:1. [PubMed: 10355547]

Cloutier M, Bolger F, Lowry J, Wellstead P. An integrative dynamic model of brain energy metabolism using in vivo neurochemical measurements. J Comput Neurosci. 2009; 3:391.

Couto P, Meurs W, Bernardes J, de Sa JM, Goodwin J. Mathematical model for educational simulation of the oxygen delivery to the fetus. Control Eng Pract. 2002; 10:59.

D'Angelo C, Papelier Y. Mathematical modeling of the cardiovascular system and skeletal muscle interaction during excecise. ESAIM Proc. 2005; 14:72.

de Haan H, Gunn A, Gluckman P. Fetal heart rate changes do not reflect cardiovascular deterioration during brief repeated umbilical cord occlusions in near-term fetal lambs. Am J Obstet Gynecol. 1997; 176:8. [PubMed: 9024082]

Durosier L, Green G, Batkin I, Seely A, Ross M, Richardson B, Frasch M. Sampling rate of heart rate variability impacts the ability to detect acidemia in ovine fetuses near-term. Front Pediatr. 2014; 2 PMC4017161.

Ellwein L, Tran H, Zapata C, Novak V, Olufsen M. Sensitivity analysis and model assessment: mathematical models for arterial blood flow and blood pressure. Cardiovasc Eng. 2008; 8:94. [PubMed: 18080757]

Frasch M, Muller T, Hoyer D, Weiss C, Schubert H, Schwab M. Nonlinear properties of vagal and sympathetic modulations of heart rate variability in ovine fetus near term. Am J Physiol Regul Integr Comp Physiol. 2009a; 296:R702. [PubMed: 19109371]

Frasch M, Mansano R, Gagnon R, Richardson B, Ross M. Measures of acidosis with repetitive umbilical cord occlusions leading to fetal asphyxia in the near-term ovine fetus. AJOG. 2009b; 200(200):e1.

Frasch M, Muller T, Hoyer D, Weiss C, Schubert H, Schwab M. Heart rate variability analysis allows early asphyxia detection in ovine fetus. Reprod Sci. 2009c; 16:509. [PubMed: 19164481]

CIHR Author Manuscript CIHR Author Manuscript CIHR Author Manuscript

CIHR Author Manuscript CIHR Author Manuscript CIHR Author Manuscript

Frasch M, Keen A, Gagnon R, Ross M, Richardson B. Monitoring fetal electrocortical activity during labour for predicting worsening acidemia: a prospective study in the ovine fetus near term. PLoS One. 2011; 6:e22100. [PubMed: 21789218]

Frasch M, Frank B, Last M, Muller T. Time scales of autonomic information flow in near-term fetal sheep. Front Physiol. 2012; 3:378. [PubMed: 23055982]

Gold N, Frasch M, Herry C, Richardson B, Seely A, Wang X. 2015Online change-point detection for non stationary biological time series with Gaussian processes. In preparation

Gui R, Schüthe C, Bernhard S. Mathematical modeling and sensitivity analysis of arterial anastomosis in arm arteries. ZIB Report. 2015

Hunter C, Blood A, Power G. Cerebral metabolism during cord occlusion and hypoxia in the fetal sheep: a novel method of continuous measurement based on heat production. J Physiol. 2003; 552:241. [PubMed: 12878759]

Jensen A, Garnier Y, Berger R. Dynamics of fetal circulatory responses to hypoxia and asphyxia. Eur J Obstet Gynecol Reprod Biol. 1999; 84:155. [PubMed: 10428339]

Khoo M, Kronauer R, Strohl K, Slutsky A. Factors inducing periodic breathing in humans: a general model. J Appl Physiol. 1982; 53:644. [PubMed: 7129986]

Khoo M, Gottschalk A, Pack A. Sleep induced periodic breathing and apnea: a theoretical study. J Appl Physiol. 1991; 70:2014. [PubMed: 1907602]

Koos B, Chau A, Qgunyemi D. Adenosine mediates metabolic and cardiovascular responses to hypoxia in fetal sheep. J Physiol. 1995; 488:761. [PubMed: 8576865]

Kubota T, Alexander J, Itaya R, Todaka K, Sugimachi M, Sunagawa K, Nose Y. Dynamic effects of carotid sinus baroreflex on ventriculoarterial coupling studied in anesthetized dogs. Circ Res. 1992a; 70:1044. [PubMed: 1568296]

Kubota T, Chishaki H, Yoshida T, Sunagawa K, Takeshita A, Nose Y. How to encode arterial pressure into carotid sinus nerve to invoke natural baroreflex. Am J Physiol. 1992b; 263:H307. [PubMed: 1636769]

Levy M, Zieske H. Autonomic control of cardiac pacemaker activity and atrioventricular transmission. J Appl Physiol. 1969; 27:465. [PubMed: 5822553]

Liang F, Liu H. Simulation of hemodynamic responses to the Valsalva Maneuver: an integrative computational model of the cardiovascular system and the autonomic nervious system. J Physiol Sci. 2006; 56:45. [PubMed: 16779913]

Liang F, Takagi S, Himeno R. Multi-scale modeling of the human cardiovascular system with applications to aortic valvular and arterial stenoses. Med Biol Eng Comput. 2009; 47:743. [PubMed: 19198911]

Liston R, Sawchuck D, Young D. Fetal health surveillance: antepartum and intrapartum consensus guideline. J Obstet Gynecol Can. 2007; 29:53.

Low J, Panagiotopoulos C, Derrick E. Newborn complications after intrapartum asphyxia with metabolic acidosis in the preterm fetus. Am J Obstet Gynecol. 1995; 172:805. [PubMed: 7892868]

Magosso E, Ursino M. A mathematical model of CO_2 effect on cardiovascular regulation. Am J Physiol Heart Circ Physiol. 2001; 281:H2036. [PubMed: 11668065]

Mallard E, Williams C, Johnston B, Gunning M, Davis S, et al. Repeated episodes of umbilical cord occlusion in fetal sheep lead to preferential damage to the striatum and sensitize the heart to further insults. Pediatr Res. 1995; 37:707. [PubMed: 7651753]

Olufsen M, Tran H, Ottesen J. Modeling cerebral blood flow control during posture change from sitting to standing. Cardiovasc Eng Int J. 2004; 4:47.

Olufsen M, Ottesen J, Tran H, Ellwein L, Lipsitz L, Novak V. Blood pressure and blood flow variation during postural change from sitting to standing: model development and validation. J Appl Physiol. 2005; 99:1523. [PubMed: 15860687]

Orlowski P, Chappell M, Park C, Grau V, Payne S. Modeling of pH dynamics in brain cells after stroke. Interface Focus. 2011; 1:408. [PubMed: 22419985]

Quilligan E, Vasicka A, Aznar R, Lipsitz P, Moore T, Bloor BM. Partial pressure of oxygen in the intervillous space and the umbilical vessels. Am J Obstet Gynecol. 1960; 79:1048. [PubMed: 14435558]

CIHR Author Manuscript CIHR Author Manuscript CIHR Author Manuscript

Ramsay J, Hooker G, Campbell D, Cao J. Parameter estimation for differential equations: a generalized smoothing approach. J R Stat Soc B. 2007; 69:741.

Ross M, Jessie M, Amaya K, Matushewski B, Durosier L, Martin M, Richardson B. Correlation of arterial fetal base deficit and lactate changes with severity of variable heart rate decelerations in the near-term ovine fetus. Am J Obstet Gynecol. 2013; 208:e1.

Shi Y, Patricia L, Rodney H. Review of zero-D and 1-D models of blood flow in the cardiovascular system. Biomed Eng Online. 2011; 10:1. [PubMed: 21244718]

Thakor A, Giussani D. Effects of acute acidemia on the fetal cardiovascular defense to acute hypoxemia. Am J Physiol Regul Integr Comp Physiol. 2008; 296:R90. [PubMed: 18922958]

Ursino M. Interaction between carotid baroregulation and the pulsating heart: a mathematical model. Am J Physiol. 1998; 275:H1733. [PubMed: 9815081]

Ursino M, Magosso E. Acute cardiovascular response to isocapnic hypoxia. I. A mathematical model. Am J Physiol Heart Circ Physiol. 2000; 279:H149. [PubMed: 10899052]

Ursino M, Magosso E. Role of short-term cardiovascular regulation in heart period variability. a modeling study. Am J Physiol Heart Circ Physiol. 2003; 284:H1479. [PubMed: 12595291]

van der Hout-van der Jagt M, Oei S, Bovendeerd P. A mathematical model for simulation of early decelerations in cardiotocogram during labor. Med Eng Phys. 2012; 34:579. [PubMed: 22041128]

van der Hout-van der Jagt M, Oei S, Bovendeerd P. Simulation of reflex late decelerations in labor with a mathematical model. Early Hum Dev. 2013; 89:7. [PubMed: 22840604]

Wang X, Durosier L, Ross M, Richardson B, Frasch M. Online detection of fetal acidemia during labour by testing synchronization of EEG and heart rate: a prospective study in fetal sheep. PLoS One. 2014; 9 PMC4182309.

Westgate J, Bennet L, Gunn A. Fetal heart rate variability changes during brief repeated umbilical cord occlusion in near term fetal sheep. J Obstet Gynecol. 1999; 106:664.

Westgate J, Bennet L, de Haan H, Gunn A. Fetal heart rate overshoot during repeated umbilical cord occlusion in sheep. Obstet Gynecol. 2001; 97:454. [PubMed: 11239656]

Westgate J, Wibbens B, Bennet L, Wassink G, Parer J, Gunn A. The intrapartum deceleration in center stage: a physiologic approach to the interpretation of fetal heart rate changes in labor. Am J Obstet Gynecol. 2007; 197(236):e1.

Yan E, Baburamant A, Walker A, Walker D. Changes in cerebral blood flow, cerebral metabolites, and breathing movements in the sheep fetus following asphyxia produced by occlusion of the umbilical cord. Am J Physiol Regul Integr Comp Physiol. 2009; 297:R60. [PubMed: 19403864]

CIHR Author Manuscript
CIHR Author Manuscript
CIHR Author Manuscript

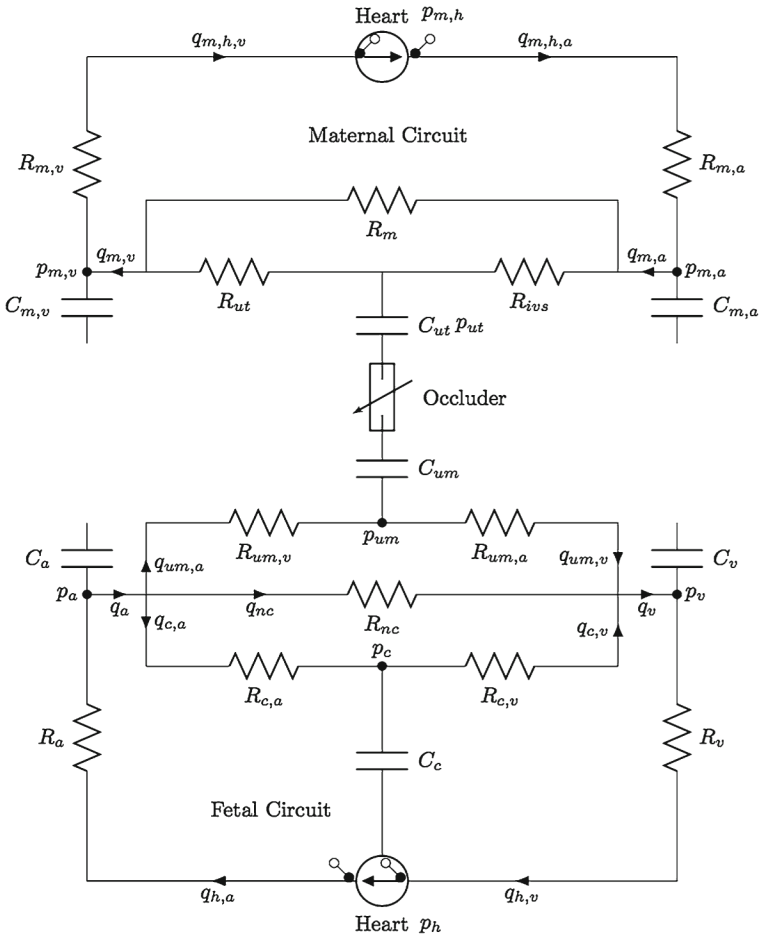

Fig. 1.

Illustration of model setup. Our model includes two circulatory networks: maternal circulation (*top*) and fetal (*bottom*) circulations. Resistors R and compliances C are indicated, *arrows* giving blood flow direction, similar to van der Hout-van der Jagt et al. (2012). In this sketch, ‘a’ stands for artery, ‘v’ for vein, ‘um’ for umbilical cord, ‘m’ for mother systemic part, ‘nc’ for fetal systemic part, c’ for cerebral part, ‘ut’ for uterine and ‘ivs’ for intervillous space

CIHR Author Manuscript

CIHR Author Manuscript

CIHR Author Manuscript

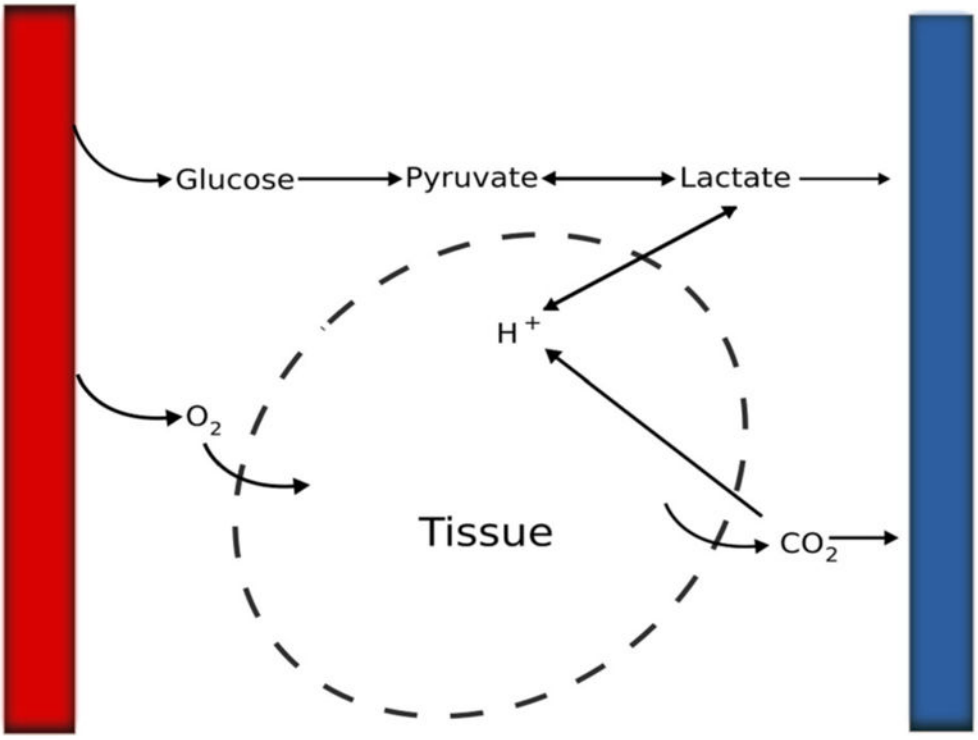

Fig. 2.

Illustration of the simplified metabolic process in certain compartment in the model. *Left* (*right*) column stands for artery (vein)

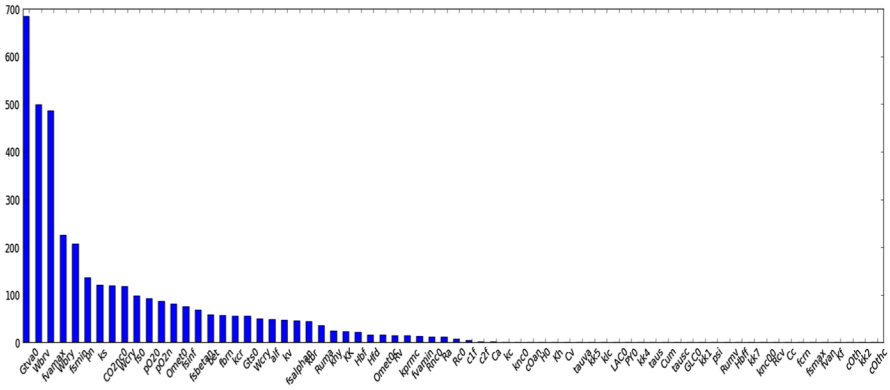

Fig. 3.

Results of sensitivity for 70 selected parameters used in the model. The *vertical axis* is calculated based on Eq. 54

CIHR Author Manuscript
CIHR Author Manuscript
CIHR Author Manuscript

CIHR Author Manuscript
CIHR Author Manuscript
CIHR Author Manuscript

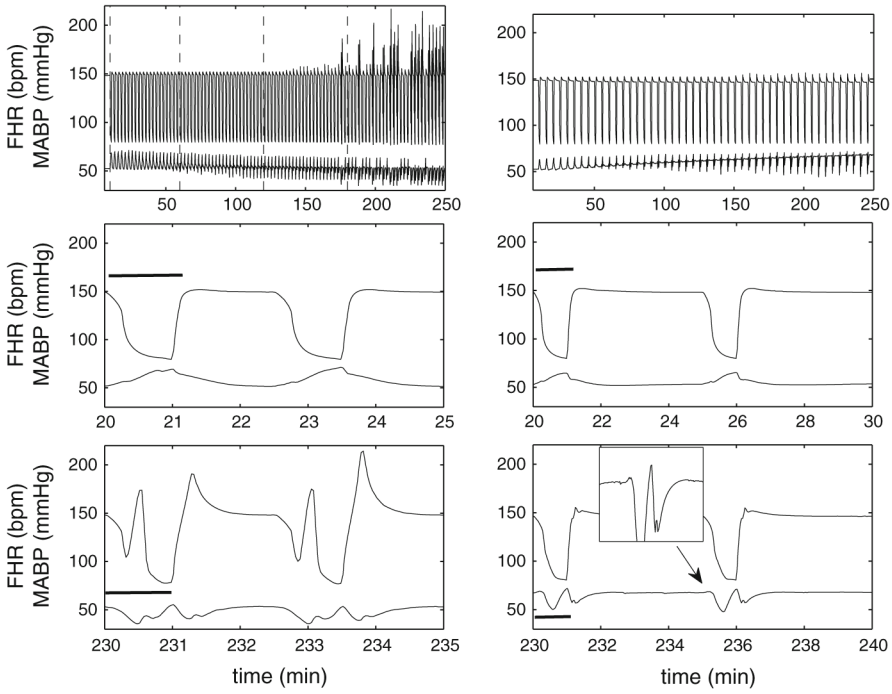

Fig. 4.

Numerical results of FHR and MABP for 1:2.5 and 1:5 UCO. Numerical results for 4 h of occlusions with 1:2.5 UCO (*left*) and 1:5 UCO (*right*). $G_c = 0.27$ and $G_{va} = -0.67$ are used in simulation with 1:5 UCO. The *dashed lines* in the *upper left panel* divide the time periods into four one-hour windows. The first *dashed line marks* the beginning of the occlusions. The *middle row* displays a zoom of 5- (*left*) and 10-min (*right*) windows for each case at the beginning of the occlusion, and the bottom row 5- (*left*) and 10-min (*right*) windows near the end of occlusions. The *black bar* indicates the occlusion duration. The *inset* of the *right bottom panel* shows that MABP rises slightly at the beginning of each occlusion and then declines

CIHR Author Manuscript
CIHR Author Manuscript
CIHR Author Manuscript

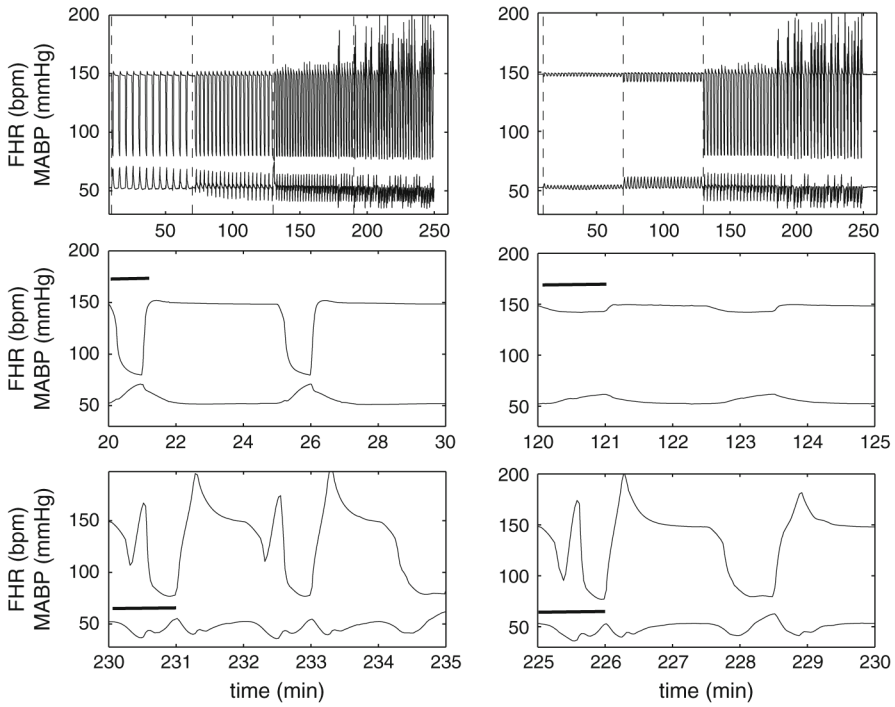

Fig. 5.

Numerical results of FHR and MABP for variable UCO. *Left panel* Complete UCO with varying occlusion frequency (1:5 UCO for the first, 1:3 for second and 1:2 for the third and fourth hours). *Right panel* Constant frequency UCOs with varying occlusion degree (mild occlusion during the first, moderate during the second and severe during the third and fourth hours). *Dashed lines* are inserted to divide the periods into four windows, each representing 1 h. The *left dashed line marks* the beginning of occlusions. The *middle row* represents 5-min windows at the beginning of the occlusion, and the *bottom row* 5-min windows near the end of occlusions. The *black bar* indicates the occlusion duration

CIHR Author Manuscript

CIHR Author Manuscript

CIHR Author Manuscript

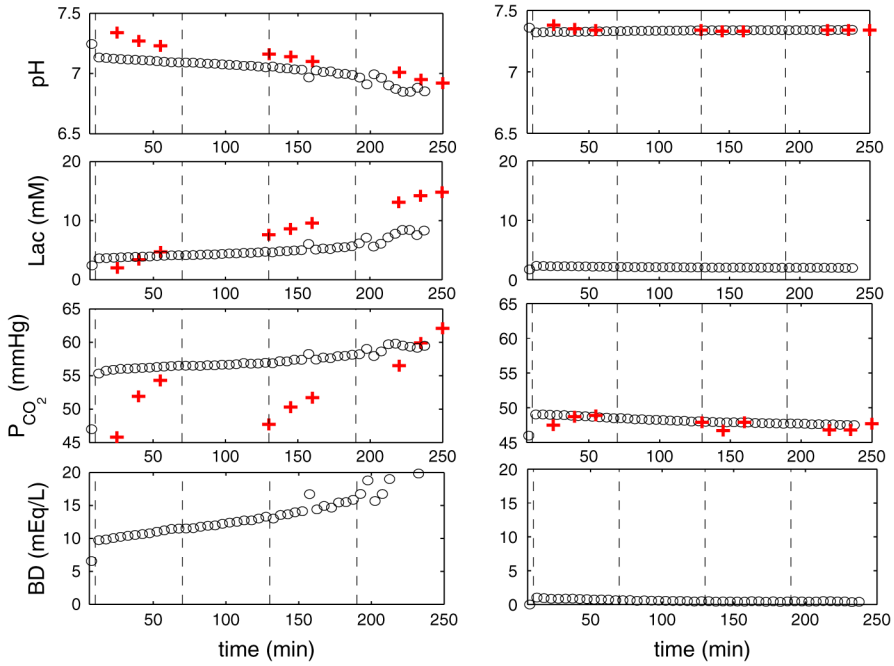

Fig. 6.

(Color figure online) Numerical results of pH, lactate, P_{CO_2} and BD for 1:2.5 and 1:5 UCO. Time variations of pH, lactate, P_{CO_2} in the systemic compartment and BD for 1:2.5 UCOs (*left*) and 1:5 UCO (*right*). The *circle symbol* represents the mean values over 5 min after occlusion begins. The *plus symbol* represents experimental data (Table 1 in Bennet et al. 2005)

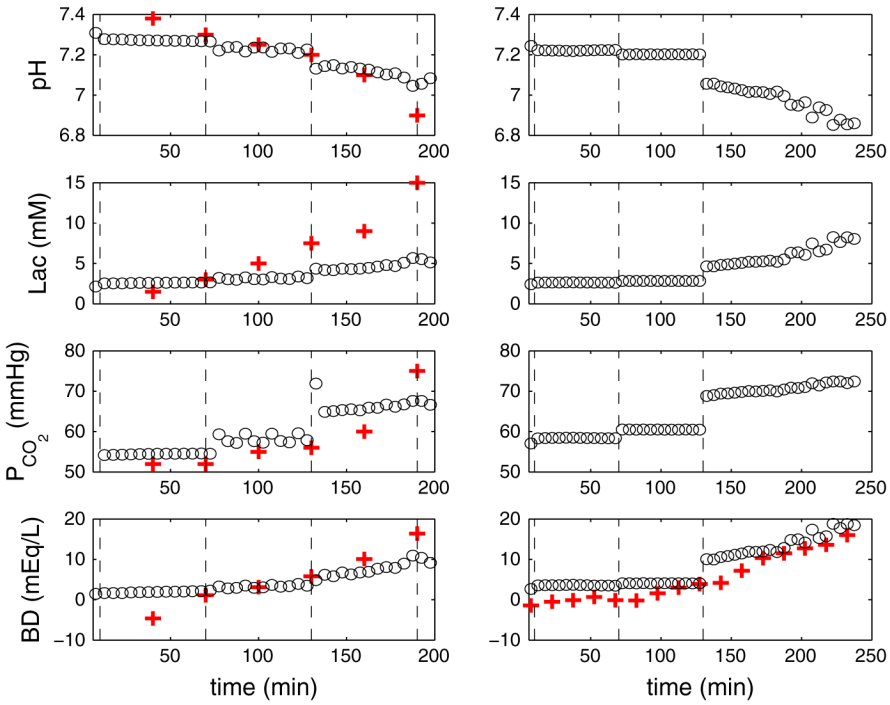

Fig. 7.

(Color online) Numerical results of pH, lactate, P_{CO_2} and BD for variable UCOs. Time variations of pH, lactate, P_{CO_2} and BD in the systemic compartment for complete UCO with varying frequency (*left column* 1:5 UCO for the first, 1:3 for second and 1:2 for the third and fourth hours) and UCO of varying degree with constant frequency (*right column* mild occlusion during the first, moderate during the second and severe during the third and fourth hours). In the simulations displayed by the *left column*, $K_7 = 35 \times 10^{-6}$ s^{-1} in Eq. 31 and $K_6 = 5$ s^{-1} are chosen to match with the experimental pH variation; $k_{CO_2} = 0.008$ in Eq. 23 is chosen to match the baseline value of $P_{CO_2} = 52.7 \pm 0.9$ mmHg in the experiments (Frasch et al. 2009b). The remaining parameters are given in Tables 1, 2 and 3

CIHR Author Manuscript CIHR Author Manuscript CIHR Author Manuscript

CIHR Author Manuscript
CIHR Author Manuscript
CIHR Author Manuscript

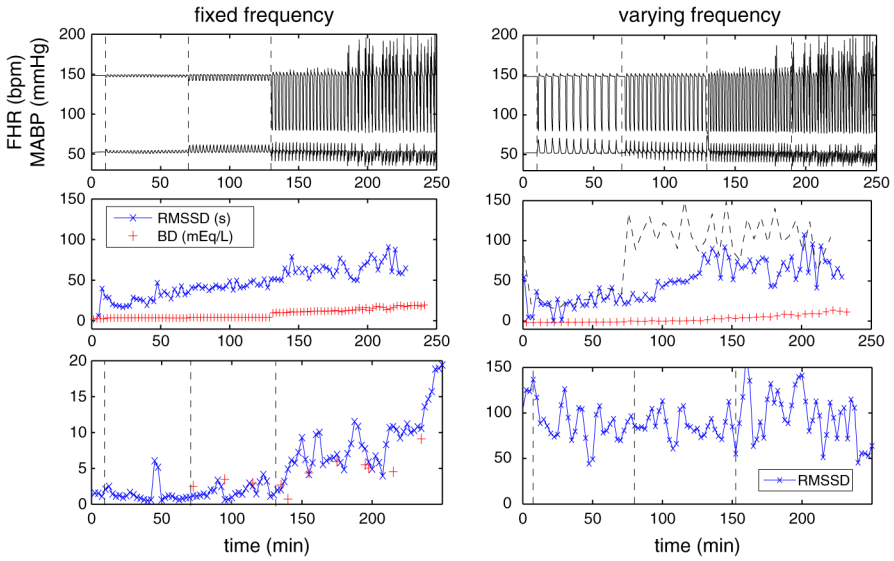

Fig. 8.

(Color figure online) Computed RMSSD with a sampling frequency of 4 Hz and BD for UCOs with varying occlusion degrees (*left*) and varying frequencies (*right*). Patterns of FHR (*top*), RMSSD and BD (*middle*), and the corresponding representative experimental results (Gold et al. 2015; Wang et al. 2014) (*bottom*). In the *middle row*, RMSSD is computed using 5-min windows for the *left column*. For the *right column*, RMSSD is computed using both 3- (*cross-symbol*) and 5-min (*dashed line*) windows

CIHR Author Manuscript
CIHR Author Manuscript
CIHR Author Manuscript

Table 1

Parameter values for cardiovascular model

Parameter	Value	Parameter	Value
a_h (mmHg/ml^2)	0.0003	b_h (ml)	6.3041
c_h (mmHg/ml)	0.9	$c_{h,m}$ (mmHg/ml)	1.5
$d_{h,m}$ (mmHg)	1.1264	d_h (mmHg)	5
ψ (1/s)	0.05	H_m (1/s)	0.9
n	5.9717	m	4.0917
$p_{\max}$ (mmHg)	1.2028	$p_{\min}$ (mmHg)	1.0994
$t_{\max}$ (s)	0.2653	$t_{\min}$ (s)	0.0801
η	19.0681	ϕ (1/s)	1.3296
θ (1/s)	1.1364	ν	9.1682
$C_{m,a}$ (ml/mmHg)	5.6	$C_{m,v}$ (mmHg s/ml)	112
C_a (ml/mmHg)	0.8	C_v (mmHg s/ml)	3.5
C_{um} (ml/mmHg)	1.1	C_c (mmHg s/ml)	0.057
$R_{m,a}$ (mmHg s/ml)	0.05	$R_{m,v}$ (mmHg s/ml)	0.025
R_{ivs} (mmHg s/ml)	3.38	R_{utv} (mmHg s/ml)	0.675
R_a (mmHg s/ml)	0.045	R_v (mmHg s/ml)	0.27
$R_{um,a}$ (mmHg s/ml)	5.236	$R_{\text{um,v}}$ (mmHg s/ml)	0.015
R_m (mmHg s/ml)	0.45	$R_{\text{nc,0}}$ (mmHg s/ml)	1.5
$R_{c,v}$ (mmHg s/ml)	0.015	$R_{c,a,0}$ (mmHg s/ml)	10.485

CIHR Author Manuscript
CIHR Author Manuscript
CIHR Author Manuscript

Table 2

Parameter values for regulation model

Parameter	Value	Parameter	Value
$R_{nc,min}$ (mmHg s/ml)	0	$R_{nc,max}$ (mmHg s/ml)	11.25
$R_{c,min}$ (mmHg s/ml)	10.485	$R_{c,max}$ (mmHg s/ml)	1.0485
T_0 (s)	0.406	$T_{va,0}$ (s)	0.373
$T_{s,0}$ (s)	−0.177	τ_0 (s)	0.21
$f_{br,min}$ (1/s)	2.52	$f_{br,max}$ (1/s)	47.78
$f_{cr,min}$ (1/s)	1.16	$f_{cr,max}$ (1/s)	17.07
$f_{hy,min}$ (1/s)	0	$f_{hy,max}$ (1/s)	2.5
$f_{va,min}$ (1/s)	3.2	$f_{va,max}$ (1/s)	6.3
$f_{s,min}$ (1/s)	2.66	$f_{s,max}$ (1/s)	60
$f_{s,0}$ (1/s)	16.11	$f_{s,\infty}$ (1/s)	2.1
$f_{cr,n}$ (1/s)	11	$f_{br,n}$ (1/s)	25
$f_{s,1}$ (1/s)	1	$f_{s\alpha,n}$ (1/s)	9
$f_{va,n}$ (1/s)	10	$f_{s\beta,n}$ (1/s)	5.5
$f_{va,o}$ (1/s)	−0.68	$\tau_{pr,br}$ (mmHg)	4.09
$\tau_{pr,cr}$ (mmHg)	7.24	τ_{Rc} (mmHg s/ml)	10
τ_{gs} (1/s)	0.05	τ_{gv} (1/s)	0.04
$\tau_{br(cr)}$ (s)	2	$\tau_{T,v}$ (s)	1.5
$\tau_{T,s}$ (s)	6	τ_s (s)	30
$k_{R_{nc}}$ (1/s)	1.44	$k_{pr,s}$ (mmHg)	2
k_c	0.018	k_{hy} (mmHg)	1.7
k_{br} (1/s)	4.09	k_{cr} (1/s)	7.24
k_s (1/s)	0.0675	k_v (1/s)	7.06
$W_{cr,va}$	0.2	$W_{br,va}$	1
$W_{br,s\beta}$	1	$W_{cr,s\beta}$	1
$W_{br,s\alpha}$	1	$W_{cr,s\alpha}$	1
$G_{T,s}$ (s^2)	−0.13	$G_{T,va,0}$ (s^2)	0.04
$G'_{T,s}$ (s^2)	0.046	δG_T (s^2)	0.1235
G_c (mmHg s/ml)	0.27	G_{va} (mmHg s/ml)	−0.17

CIHR Author Manuscript
CIHR Author Manuscript
CIHR Author Manuscript

Table 3

Parameter values for metabolic model

Parameter	Value	Parameter	Value
α_b (ml O_2/g Hb)	1.34	β_d (ml O_2/ml blood/mmHg)	0.0031
Hb_m (g Hb/ml blood)	12×10^4	Hb_f (g Hb/ml blood)	17×10^4
$c_{1,m}$ (mmHg^3)	23,400	$c_{2,m}$ (mmHg^2)	150
$c_{1,f}$ (mmHg^3)	10,400	$c_{2,f}$ (mmHg^2)	150
$[O_2]_{a,n}$ (ml O_2/ml blood)	0.04	$P_{CO_2,n}$ (mmHg)	44
$P_{O_2,0,c}$ (mmHg)	7	$[O_2]_{th}$ (ml O_2/ml blood)	0.068
$P_{O_2,a,n}$ (mmHg)	7.5	K_{th} (ml blood/s)	9.33
K_{CO_2} (ml CO_2/ml blood/mmHg)	0.244	k_{CO_2} (ml CO_2/ml blood)	0.007
D_{CO_2} (ml CO_2/s/mmHg)	0.1	D (ml O_2/s/mmHg)	0.0283
$[GL]_a$ (mM)	1	$[LA]_a$ (mM)	0.8
$[Py]_a$ (mM)	0.12	$[H^+]_a$ (nM)	40
K_1 (mmol/s)	100	K_2 (ml/s)	40
K_3 (ml/s)	0.4	K_4 (ml/s)	4
K_5 (ml/s)	0.5	K_6 (ml/s)	10
K_7 (10^{-6} ml/s)	55	K_8 (nmol/s)	10
K_9 (nmol/s)	15	K_{10} (10^6 ml/s)	0.2

CIHR Author Manuscript

CIHR Author Manuscript

CIHR Author Manuscript

Table 4

Clinically relevant quantities for the baseline case in feuts

Physical quantity	Reference/target value	Model output
FHR (bpm)	135 (van der Hout-van der Jagt et al. 2012), 163 ± 5 (Frasch et al. 2011)	148
Mean fetal arterial $\bar{p}_a$ (mmHg)	55 ± 5 (Bennet et al. 2005), 46 ± 2 (Hunter et al. 2003)	52.5
Umbilical P_{O_2} (mmHg)	18 (van der Hout-van der Jagt et al. 2012)	17.6
Cerebral P_{O_2} (mmHg)	10 ± 1 (Bishai et al. 2003)	12.3
Systemic P_{CO_2} (mmHg)	45.5 ± 2 (Bennet et al. 2005) 52.7 ± 0.9 (Frasch et al. 2009c, 2011)	47.5
Intervillous space P_{O_2} (mmHg)	23.3 (van der Hout-van der Jagt et al. 2012; Quilligan et al. 1960)	23.2
Systemic lactate (mM)	1.6 ± 0.2 (Frasch et al. 2009c)	2.1
Systemic pH	7.36 ± 0.1 (Frasch et al. 2009c), 7.4 ± 0.01 (Bennet et al. 2005)	7.25

CIHR Author Manuscript

CIHR Author Manuscript

CIHR Author Manuscript

Table 5

Descriptions of the top 10 most sensitive parameters in the model in decreasing order

Parameter	Role	Effect
$G_{T,\mathrm{va},0}$	Vagal gain	Increase the contribution to heart period by vagal activity
$W_{\mathrm{br,va}}$	Weight factor in f_{va} in (39)	Increase the contribution due to baroreflex in vagal firing rate
$f_{\mathrm{va,max}}$	Maximum in sigmoid curve due to baroreflex	Increase f_{va} in (39)
$W_{\mathrm{br},s\beta}$	Factor in front of f_{br} in (42)	Decrease $f_{s\beta}$
$f_{\mathrm{s,min}}$	Threshold in (40)	Increase the inactive range f_s
P_n	Threshold to trigger baroreceptor in (44)	Reduce the time to obtain the FHR overshoot
k_{s}	Factor in the exponent of (42)	Increase the steepness of sigmoid curve in (42)
$W_{\mathrm{cr,va}}$	Weight factor in front of f_{cr} in (39)	Increase f_{va}
$f_{\mathrm{s},0}$	Factor in (42)	Increase $f_{s\alpha(\mathrm{s}\beta)}$
$P_{\mathrm{O}_2,c,0}$	Threshold to trigger chemoreceptor in (41)	Promote the chemoreflex

CIHR Author Manuscript

CIHR Author Manuscript

CIHR Author Manuscript

Table 6

Contingency tables for 1:2.5 UCO

	***Y* = 0**	***Y* = 1**	***Y* = 0**	***Y* = 1**	***Y* = 0**	***Y* = 1**
X = 0	3303	266	3167	251	3204	31
X = 1	4	27	140	42	103	262

X stands for the binary series for FHR, MABP and lactate from left to right, whereas *Y* stands for BD

CIHR Author Manuscript

CIHR Author Manuscript

CIHR Author Manuscript

Table 7

Contingency tables for UCO with various frequencies

	***Y* = 0**	***Y* = 1**	***Y* = 0**	***Y* = 1**	***Y* = 0**	***Y* = 1**
X = 0	3250	324	3137	304	3151	74
X = 1	4	22	117	42	103	272

X stands for the binary series for FHR, MABP and lactate from left to right, whereas *Y* stands for BD

CIHR Author Manuscript

CIHR Author Manuscript

CIHR Author Manuscript

Table 8

Contingency tables for UCO with various degrees

	$Y = 0$	$Y = 1$	$Y = 0$	$Y = 1$	$Y = 0$	$Y = 1$
$X = 0$	3220	376	3135	372	3118	92
$X = 1$	2	2	87	6	104	286

X stands for the binary series for FHR, MABP and lactate from left to right, whereas Y stands for BD